DOI: 10.1002/adma.200702770

Dendrimer-Functionalized Shell-crosslinked Iron Oxide Nanoparticles for In-Vivo Magnetic Resonance Imaging of Tumors**

By *Xiangyang Shi,* Su He Wang,* Scott D. Swanson, Song Ge, Zhengyi Cao, Mary E. Van Antwerp, Kevin J. Landmark,* and *James R. Baker, Jr.**

Non-invasive diagnosis and detection of early-stage tumors is regarded as one of the current challenges in the biomedical sciences. Magnetic resonance (MR) imaging is a powerful, non-invasive imaging technique because of its high spatial resolution and tomographic capabilities. However, the signal sensitivity of MR imaging for specific biological targets is largely dependent on the specificity and selectivity of the ligand used to target magnetic nanoparticles (NPs) to specific tissues. Development of tumor-targeted magnetic NPs is necessary to enhance the MR signal sensitivity for in-vivo tumor detection. Various proteins such as transferrin,[1,2] anti-carcinoembryonic antigen monoclonal antibody rch 24,[3] herceptin,[4–6] and chlorotoxin[7] have been conjugated onto iron oxide NP surfaces. Unfortunately, these protein ligands tend to display immunogenecity and the biological macromolecules used are very expensive and not available for many types of cancer, which thereby limits their applications. One of the most widely used cancer-targeting ligands is folic acid (FA), which targets FA receptors (FAR) that are overexpressed in several human carcinomas including breast, ovary, endometrium, kidney, lung, head and neck, brain, and myeloid cancers.[8–10] Several groups have investigated the conjugation of folic acid (FA) onto iron oxide NPs for targeting tumor cells.[11–17] However, many of these reports are limited to in-vitro studies. This is largely a result of difficulties related to the in-vivo stability and macrophage uptake of many FA-modified magnetic NPs. It implies that a biocompatible and robust polymer coating onto iron oxide NP surfaces may be essential for a successful in-vivo MR imaging of a tumor.

The authors have recently embarked on the surface modification of iron oxide NPs with dendrimers for biomedical imaging applications. Dendrimers are a new class of highly branched, monodispersed, and synthetic macromolecules with well-defined structure, composition, and architecture. Dendrimers, especially poly(amidoamine) (PAMAM) dendrimers, have been shown to be capable of conjugating targeting ligands, imaging agents, and drug molecules for targeted cancer therapeutics.[18–21] It is expected that appropriately manipulating the iron oxide NP surfaces with dendrimer chemistry may offer possibilities for sensing of various biological systems. Early work has shown that carboxy-terminated PAMAM dendrimers can be successfully assembled onto Fe_3O_4 NPs for intracellular uptake studies.[22] However, because of the large amount of carboxy groups on the dendrimer surface, the Fe_3O_4 NPs modified with FA do not show specific binding to the FAR-expressing cells in vitro. In a previous work, it has been shown that Fe_3O_4 NPs modified through an approach that combines a layer-by-layer (LbL) self-assembly technique[23–34] and dendrimer chemistry[18–20] can specifically target tumor cells overexpressing FAR in vitro.[35] In these studies, a bilayer composed of polystyrene sulfonate sodium salt (PSS) and FA- and FI (fluorescein isothiocyanate)-functionalized PAMAM dendrimers of generation 5 ($G5.NH_2$-FI-FA) were assembled onto Fe_3O_4 NPs through electrostatic LbL assembly, followed by acetylation of the remaining surface amine groups of the assembled G5 dendrimers. Unfortunately, in-vivo data show that most of these bilayer-modified Fe_3O_4 NPs accumulate in the liver of mice, which suggests that the particles lack in-vivo stability (unpublished results). Development of a robust polymer shell coating onto Fe_3O_4 is necessary to achieve a successful in-vivo MR image of a tumor. Approaches to accomplish this involve increasing the polymer layer thickness and/or chemically crosslinking the polymer shells.[36–41]

Literature reports show that poly(glutamic acid) (PGA) and poly(L-lysine) (PLL) multilayers can be successfully self-assembled on planar substrates[42,43] and display very good biocompatibility for implant coatings.[44] In this present study, iron oxide NPs are assembled with multilayers of PGA and PLL, followed by assembly with $G5.NH_2$-FI-FA dendrimers. The interlayers are then crosslinked through EDC

[*] Dr. X. Shi, Dr. S. H. Wang, Z. Cao, M. E. Van Antwerp
Prof. J. R. Baker, Jr.
Michigan Nanotechnology Institute for Medicine and Biological Sciences
University of Michigan, Ann Arbor, MI 48109 (USA)
E-mail: xshi@umich.edu; shidasui@umich.edu; jbakerjr@umich.edu
Dr. S. D. Swanson
Department of Radiology
University of Michigan, Ann Arbor, MI 48109 (USA)
S. Ge, K. J. Landmark
Department of Physics
University of Michigan, Ann Arbor, MI 48109 (USA)

[**] X. Shi and S. H. Wang contributed equally to this work. This project has been funded in whole or in part by the National Institutes of Health (NIH) (under the contract # NIH 1 RO1 EB002657, NOI-CO-97111, and NIH 1 RO1 CA119409) and the Michigan Economic Development Corporation-Life Sciences Corridor Fund (under award GR-472). The authors thank Sasha Meshinchi for his assistance with the TEM experiments and valuable discussions. Supporting Information is available online from Wiley InterScience or from the author.

ADVANCED MATERIALS

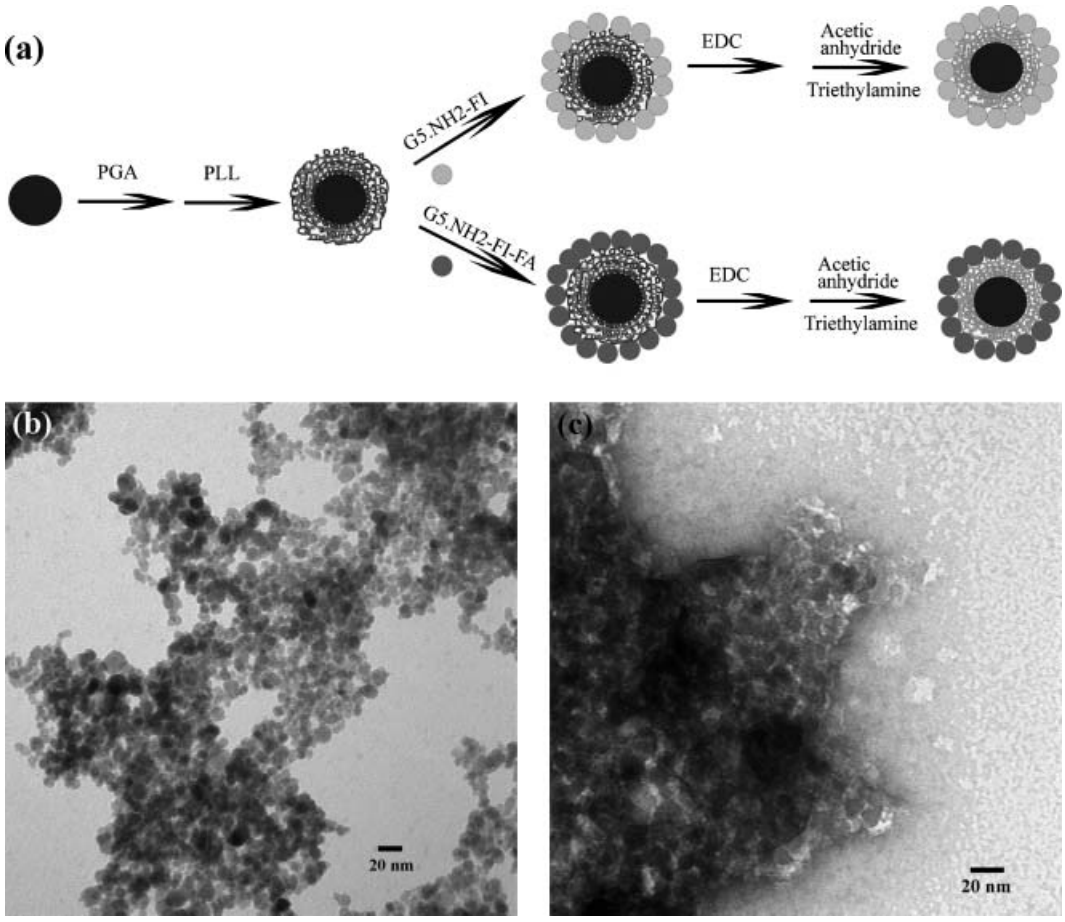

Figure 1. a) Schematic representation of the procedure for fabricating multifunctional shell-crosslinked iron oxide NPs. b) A TEM image of SCIO-FA NPs. c) A negatively phosphotungstic acid-stained TEM image of SCIO-FA NPs.

(1-ethyl-3-[3-dimethylaminopropyl]carbodiimide hydrochloride) chemistry to covalently link the hydroxy groups of iron oxide, the carboxy groups of PGA, and the amino groups of PLL and the dendrimers. The remaining amino groups of the dendrimers are finally acetylated to neutralize the surface charge (Fig. 1a). The formed shell-crosslinked iron oxide (SCIO) NPs are characterized using zeta-potential analysis, Fourier-transform infrared (FT-IR) spectroscopy, transmission electron microscopy (TEM), and relaxivity measurements. Combined flow cytometry and in-vitro and in-vivo MR imaging studies show that the FA-modified SCIO NPs can specifically bind to tumor cells and an early-stage tumor model overexpressing FAR. To our knowledge, this is the first example of the fabrication of multifunctional iron oxide NPs using shell-crosslinked polymer multilayers combined with dendrimer chemistry for in-vivo MR imaging studies. The present approach using crosslinked polymer shells to functionalize Fe_3O_4 NPs with biological ligands opens a new avenue to fabricating various NPs for a range of in-vivo biological sensing and therapeutic applications.

LbL self-assembly, shell crosslinking, and chemical modification of the SCIO NPs were monitored by zeta-potential measurement (Table S1, Supporting Information). It is clear that the positively charged Fe_3O_4 NPs become negatively charged after PGA modification. After PLL assembly, the Fe_3O_4 NPs again reverse to being positively charged. Further PGA modification decreases the surface charge. The changes in charge of the Fe_3O_4 NPs indicate the successful electrostatic assembly of $(PGA/PLL)_2/PGA/G5.NH_2$-FI-FA multilayers. The EDC crosslinking reaction does not result in a significant change of the surface charge of the Fe_3O_4 NPs. However, after the acetylation reaction, the zeta potentials of both $(PGA/PLL)_2/PGA/G5.NHAc$-FI and $(PGA/PLL)_2/PGA/G5.NHAc$-FI-FA NPs are close to neutral because of the conversion of the dendrimer surface amine groups to acetamide groups. This is in sharp contrast to the findings in a previous work,[35] wherein acetylation of dendrimer/PSS bilayer-modified Fe_3O_4 NPs did not result in Fe_3O_4 NPs with close to a neutral charge. This is presumably a result of the EDC crosslinking reaction, which makes the dendrimer amines that interact with the PGA polymer through electrostatic interaction covalently couple with the PGA.

The fabricated SCIO NPs were characterized by TEM (Fig. 1b and 1c). The morphology of the FA-modified SCIO

(SCIO-FA) NPs does not show significant change after the assembly and crosslinking of the polymers and dendrimers when compared with the pristine Fe_3O_4 NPs (Fig. 1b).[22,35] A negatively stained TEM image using phosphotungstic acid (Fig. 1c) clearly shows that all Fe_3O_4 NPs are surrounded with the bright rings of the polymer multilayers, which confirms the successful self-assembly process. The non-targeted SCIO (SCIO-NonFA) NPs display a morphology similar to that of SCIO-FA NPs (images not shown). The fabricated SCIO NPs are very stable both in aqueous solution and in a cell culture medium for at least 6 months at Fe concentrations of up to 10 mg mL^{-1}. It is worth noting that five layers of the polyelectrolyte (PGA and PLL) were selected to deposit onto the Fe_3O_4 NPs in this work. This is because the assembly of five layers of polyelectrolytes plus one layer of G5 dendrimers is sufficient to maintain the shape of the intact hollow polymer capsules once the Fe_3O_4 core particles are removed (see below in Fig. 2). This is also consistent with previous reports related to the formation of polyelectrolyte multilayer capsules.[25,45] It is likely that fewer layers of the PGA/PLL assembly may result in a weak stability of the SCIO NPs for in-vivo applications, while the assembly of more PGA/PLL layers might introduce issues related to the colloidal stability of the SCIO NPs as discussed in a previous report.[35]

The EDC chemical crosslinking reaction was confirmed by FT-IR spectrometry (Supporting Information, Fig. S1). The absorbance of the amide bond of $(PGA/PLL)_2$/PGA/G5.NH_2-FI-FA-modified Fe_3O_4 NPs increased after EDC crosslinking when compared with the same NPs before EDC crosslinking. Although FT-IR spectroscopy is not a very effective approach to characterize the intensity of the amide bond before and after shell crosslinking (because the PGA and PLL polymers, and the dendrimers that were used themselves, also contain many amide bonds), the FT-IR spectra qualitatively verify the formation of amide bonds between the carboxy groups of PGA and the amine groups of PLL and dendrimers. To further confirm the improvement of the mechanical stability after EDC shell crosslinking, the morphology of the polymer shells after the removal of the iron oxide core particles was investigated (Fig. 2). It is clear that before EDC crosslinking, intact hollow polymer nanocapsules can be formed (Fig. 2a–c). Some of the capsules have a completely empty interior (Fig. 2b), while some of the capsules still contain iron residue as a result of incomplete removal (Fig. 2c). In sharp contrast, after EDC crosslinking, most of the capsules formed are broken (Fig. 2d). This is presumably because of the huge rupture force induced instantaneously by the swelling and dissolution of iron oxide cores, which further confirms that the mechanical stability of the SCIO NPs is significantly improved, while the permeability of the capsules after EDC crosslinking is decreased. This provides further evidence to show the successful EDC crosslinking reaction.

The transverse relaxation time (T_2) of water protons in an aqueous solution of fabricated SCIO NPs was measured at 2 Tesla with a Carr–Purcell–Meiboom–Gill (CPMG) pulse sequence and the measured data were used to compute the transverse relaxivity (r_2) (the transverse relaxation rate per mM of iron). The r_2 of uncoated Fe_3O_4 NPs, SCIO-FA NPs, and SCIO-NonFA NPs as a function of Fe concentration are shown in the Supporting Information (Fig. S2). The uncoated Fe_3O_4 NPs show the highest r_2 relaxivity ($r_2 = 100.4\,s^{-1}\,mM^{-1}$), whereas the r_2 relaxivities of SCIO-FA and SCIO-NonFA NPs are somewhat reduced at 46.3 and 78.8 $s^{-1}\,mM^{-1}$, respectively. The polymer coating onto the Fe_3O_4 NPs shields water molecules from their surfaces, and causes the lower r_2 relaxivity of SCIO NPs. Compared with SCIO-NonFA NPs, the presence of the FA moieties of the SCIO-FA NPs may significantly increase the hydrophobicity and hindrance of the coating layers, thereby enhancing the shielding effect.[46] As a consequence, SCIO-FA NPs exhibit a lower r_2 relaxivity than that of SCIO NPs without FA.

The cytotoxicity of the functionalized SCIO NPs was evaluated by fluorescein diacetate (FDA) and propidium iodide (PI) staining. Cell viability data (Supporting Information, Fig. S3) show that the KB cells (a human epithelial carcinoma cell line) treated by SCIO NPs with or without FA conjugation display a similar percentage of FDA positive cells to the KB cells treated by unmodified Fe_3O_4 NPs at an Fe

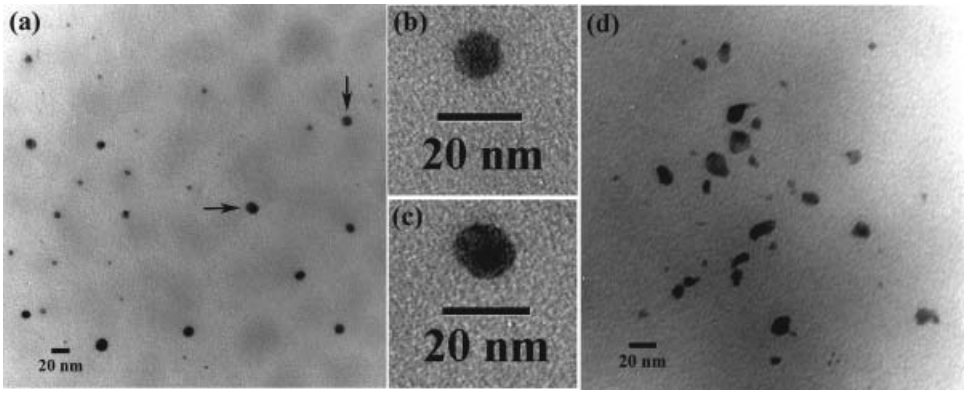

Figure 2. TEM images of $(PGA/PLL)_2$/PGA/G5.NH_2-FI-FA hollow polymer capsules after iron oxide core removal. a) $(PGA/PLL)_2$/PGA/G5.NH_2-FI-FA intact hollow polymer capsules before EDC crosslinking. b) A magnified image of the capsule indicated by a vertical arrow. c) A magnified image of the capsule indicated by a horizontal arrow. d) $(PGA/PLL)_2$/PGA/G5.NH_2-FI-FA hollow polymer capsules after EDC crosslinking.

ADVANCED MATERIALS

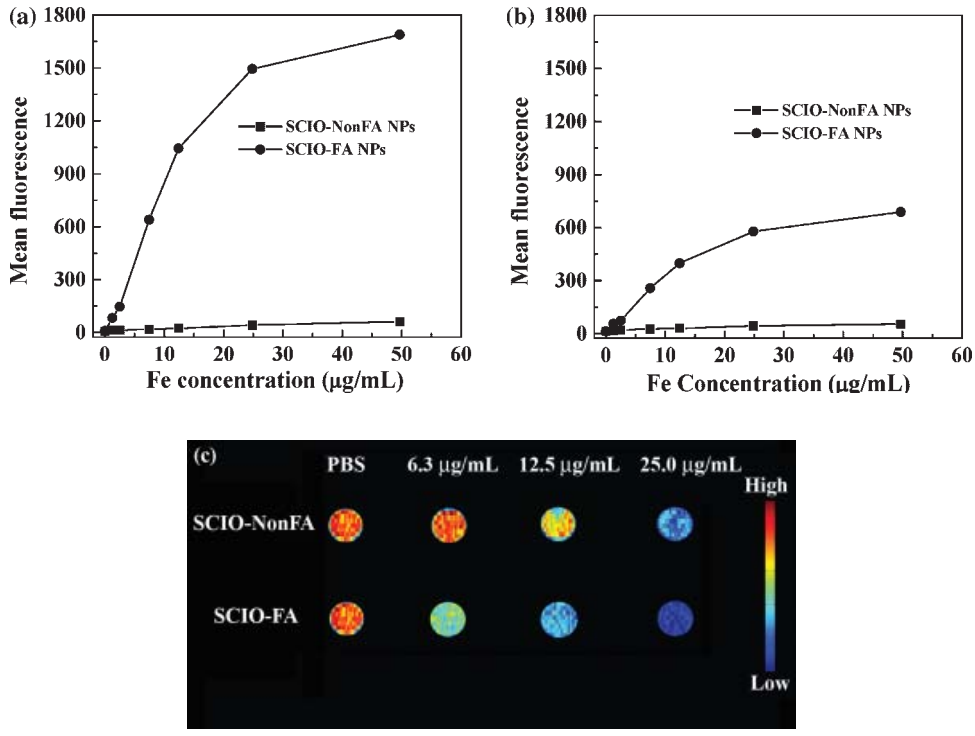

Figure 3. In-vitro flow cytometric analysis of binding of SCIO NPs with KB cells and MR images of cell pellets. Dose-dependent binding of SCIO-FA and SCIO-NonFA NPs with KB cells expressing high- (a) and low-level (b) FAR. T_2 weighted spin-echo images of KB-HFAR cells incubated with functionalized SCIO-FA and SCIO-NonFA NPs with Fe concentrations of 0, 6.3, 12.5, 25.0 μg mL^{-1} c). The color change from red to blue indicates the gradual decrease of MR signal intensity.

concentration of 0–100 μg mL^{-1}. This indicates that the SCIO NPs are biocompatible at an Fe concentration of up to 100 μg mL^{-1}.

The FA and FI dyes on the modified G5 dendrimer surfaces were used as targeting ligands and imaging molecules, respectively. The attached FI moieties afford a flow cytometric study of the binding of SCIO NPs with target cells. KB cells that express both high and low levels of FAR (denoted as KB-HFAR and KB-LFAR, respectively) were selected for the intracellular uptake of SCIO NPs. Figure 3a and 3b illustrate the dose-dependent cellular uptake of the binding of SCIO-FA and SCIO-NonFA NPs. At an Fe concentration above 2.5 μg mL^{-1}, KB-HFAR cells exposed to SCIO-FA NPs show remarkably higher fluorescence signals than those treated with SCIO-NonFA NPs without FA (Fig. 3a). With the increase of Fe concentration, the mean fluorescence levels off. This implies that the high affinity of FAR mediates specific uptake of the NPs. Both SCIO-NonFA and SCIO-FA NPs display much less uptake in KB-LFAR cells than in KB-HFAR cells, even at an Fe concentration of up to 50 μg mL^{-1} (Fig. 3b). However, in the studied concentration range, SCIO-FA NPs exhibit more uptake in KB-LFAR cells than SCIO-NonFA NPs without FA modification, which is similar to what was observed with these cells in a previous study.[35] This is a result of the larger number of FA moieties per SCIO-FA NP compared with a single FA-modified dendrimer, which facilitates polyvalent binding, thereby significantly increasing the binding affinity of Fe_3O_4 NPs to each KB-LFAR cell.

Iron oxide NPs affect the MR signal by dephasing transverse magnetization and hence reducing the value of T_2. A targeted iron oxide NP would have a major benefit in tumor imaging by specifically detecting tumors that overexpress the FAR. To study the effect of the SCIO-FA NPs on tumor cells, the T_2 of KB-HFAR cells exposed to differing Fe concentrations of SCIO-FA NPs were measured. The T_2 values of KB-HFAR cell pellets treated with SCIO-FA NPs dramatically decreased as a function of Fe concentration (Table 1). In contrast, the decreasing trend of T_2 values as a function of Fe concentration for the same KB cells treated with SCIO-NonFA NPs is significantly less than that of the KB cells treated with SCIO-FA NPs. In the T_2-weighted spin-echo MR images (the color change from red to blue indicates the gradual decrease of

Table 1. T_2 of KB-HFAR cells treated with functionalized Fe_3O_4 NPs.

Fe concentration [μg mL^{-1}]	T_2 [s]	
	SCIO-NonFA	SCIO-FA
0 (PBS control)	1.16 ± 0.016	1.16 ± 0.016
6.3	0.387 ± 0.004	0.104 ± 0.005
12.5	0.105 ± 0.006	0.062 ± 0.0009
25.0	0.061 ± 0.0001	0.03 ± 0.0014

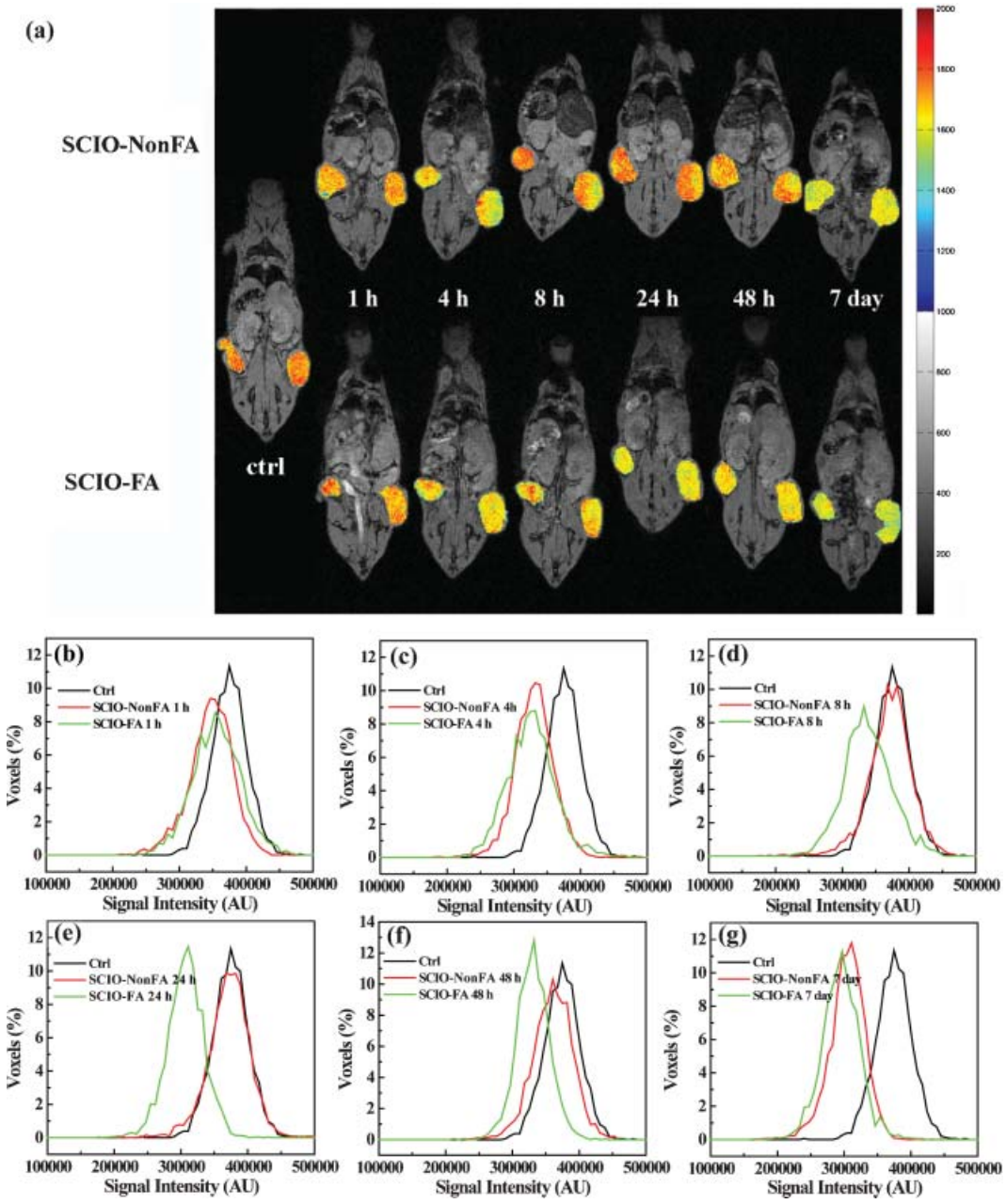

Figure 4. In-vivo MR imaging of tumor. In-vivo color maps (a) of T_2-weighted MR images of mice implanted with cancer cell line KB cells, at different time points after injection of SCIO-NonFA and SCIO-FA NPs, respectively. The color bar (from red to blue) indicates the MR signal intensity changes from high to low. Comparison of statistically normalized histograms of the voxel intensities (whole tumor) from targeted SCIO-FA (green histogram) and non-targeted SCIO-NonFA (red histogram) NPs at the time points of 1 h (b), 4 h (c), 8 h (d), 24 h (e), 48 h (f), and 7 days (g).

MR signal intensity, which is similar to those reported based on the intensity of the black color[4,47]) obtained using an Fe concentration of 25 $\mu g\,mL^{-1}$, SCIO-FA NPs significantly diminished the signal (Fig. 3c). This suggested that SCIO-FA NPs can specifically hamper the MR signal through FAR-mediated binding and endocytosis.

The in-vivo MR imaging of tumors using SCIO NPs are presented on one slice of the three-dimensional (3D) dataset from the images acquired following the injection of either targeted SCIO-FA or non-targeted SCIO-NonFA NPs (Fig. 4a). The images were colored to allow easy visualization of the contrast changes as a function of time post-injection. The control image was obtained from a mouse without treatment. The tumor MR signal intensity of mice injected with SCIO-FA NPs gradually decreases as a function of time. In sharp contrast, the tumor MR signal intensity of mice treated with SCIO-NonFA NPs does not decrease significantly with time post-injection. It is clear that 24 h after injection of the

ADVANCED MATERIALS

SCIO-FA NPs, the tumor MR signal intensity has decreased more significantly than the signal intensity in the tumors of the mouse treated with non-targeted SCIO-NonFA NPs and in the control mouse. After 48 h post-injection, the difference of the MR signal intensity of the tumors is smaller for both mice injected with SCIO-FA and SCIO-NonFA NPs. It is worth mentioning that the size of the colored tumors shown in Fig. 4a may not be consistent because the T_2-weighted MR images of the mice may be taken at different positions, and the images shown in Fig. 4a might not be in the same plane for the same mouse. The MR intensity data from the whole tumor at different slices were collected and used to create normalized statistical histograms of the signal decrease for all time points of post-injection (Fig. 4b–g). Again, it is clear that at the 24 h post-injection time point, the targeted SCIO-FA NP-treated tumor shows the most significant decrease of signal intensity when compared with the tumor treated with SCIO-NonFA NPs and the control mouse. After 48 h post-injection, the differences between the tumor MR signal intensity of the targeted and non-targeted NPs becomes smaller. The differences in the MR signal intensity of several major organs (such as the liver, kidney, muscle, and tumor) of different mice at 24 h after injection of the SCIO NPs were also compared in order to gain an understanding of the biodistribution of SCIO NPs (Fig. S4, Supporting Information). It is clear that for SCIO-FA NP-treated mice, the MR signal intensity of the tumor, kidney, and muscle decreased more significantly when compared with the control mice and the SCIO-NonFA NP-treated mice. This suggests that the SCIO-FA NP-treated mice show more iron oxide uptake in the three different tissues than the SCIO-NonFA NP-treated mice. However, the MR signal intensity of the liver follows the order of: control mice > SCIO-FA NP-treated mice > SCIO-NonFA NP-treated mice. This suggests that SCIO-NonFA NP-treated mice display more uptake of iron oxide in the liver than the SCIO-FA NP-treated mice. It is very important to note that the selection of the PGA and PLL polymer pair for the in-vivo MR imaging studies may be extended to other polymer pairs that can be chemically crosslinked. However, the polymer pairs must be biocompatible. Unpublished data show that the SCIO NPs prepared using a poly(acrylic acid)/poly(allylamine hydrochloride) multilayer assembly under similar conditions do not allow for effective MR imaging of tumors in vivo at 24 h. As a matter of fact, a slight decrease of MR signal in tumors for FA-targeted NPs (as compared with non-targeted NPs without FA modification) can only be observed after 7 days. It implies that the polymer pairs used to assemble Fe_3O_4 NPs must be biocompatible in order to avoid significant macrophage cellular uptake.

In summary, a novel approach has been developed that uniquely combines the LbL self-assembly method with dendrimer chemistry to fabricate targeted shell-crosslinked iron oxide NPs for MR imaging of tumors. The fabricated SCIO NPs are water-soluble, stable, and biocompatible. Both in-vitro and in-vivo MR imaging studies show that the SCIO NPs with FA modification (SCIO-FA NPs) can specifically target tumor cells that overexpress FAR and an FAR-expressing tumor model with a volume as small as $0.60 \pm 0.15\,cm^3$, respectively. This approach to the functionalization of magnetic NPs may be applied to other small targeting molecules (e.g., peptides and growth factors), thereby providing a general cost-effective approach for MR detection of various biological systems.

Experimental

Materials: Ethylenediamine core amine-terminated PAMAM dendrimers of generation 5 (G5.NH_2) with a polydispersity index of less than 1.08 were purchased from Dendritech (Midland, MI). FA, FI, acetic anhydride, triethylamine, ferric chloride hexahydrate ($FeCl_3{\cdot}6H_2O$ > 99%), ferrous chloride tetrahydrate ($FeCl_2{\cdot}4H_2O$ > 99%), sodium hydroxide, 2-(*N*-morpholino)ethane sulphonic acid (MES), 1-ethyl-3-[3-dimethylaminopropyl]carbodiimide hydrochloride (EDC), hydrochloric acid, and all the other chemicals and solvents were purchased from Aldrich (St. Louis, MO) and used as received. Poly(L-glutamic acid) (PGA) sodium salt ($M_w = 15\,000$–$50\,000\,g\,mol^{-1}$) and poly (L-lysine) (PLL) hydrobromide ($M_w = 15\,000$–$30\,000\,g\,mol^{-1}$) were from Sigma. Iron oxide NPs, and FI- and FA-functionalized generation 5 (G5.NH_2-FI-FA) PAMAM dendrimers were synthesized and characterized according to previously published methods [35]. FI-functionalized G5 dendrimers (G5.NH_2-FI) without FA conjugation were used as control. PGA, PLL, and dendrimers were dissolved in phosphate-buffered saline (PBS) solution (pH 7.4) that contained 0.5 M NaCl at a concentration of $1\,mg\,mL^{-1}$. KB cells were from American Type Tissue Collection (ATCC, Rockville, Maryland). Penicillin, streptomycin, fetal bovine calf serum (FBS), fluorescein diacetate (FDA), and propidium iodide (PI) were purchased from Sigma (St. Louis, MO). Trypsin-EDTA, Dulbecco's PBS, and RPMI 1640 medium (with or without FA), and bovine serum albumin were obtained from GIBCO-BRL (Gaithersburg, MD).

Fabrication of Multifunctional Shell-crosslinked Iron Oxide NPs: The procedure used to fabricate multifunctional SCIO NPs is shown in Fig. 1a. The LbL assembly of oppositely charged PGA and PLL was performed according to the literature. [27] Briefly, a solution of Fe_3O_4 NPs (5 mg in 0.5 mL water, diameter 8.4 ± 1.4 nm, synthesized and characterized according to previously published methods [35]) was added to 1 mL of a PGA solution ($1\,mg\,mL^{-1}$, pH 7.4 PBS buffer that contained 0.5 M NaCl) with occasional shaking. After adsorption of PGA for 20 min, the suspension was centrifuged at 8000 rpm for 10 min. The supernatant was then carefully removed, and the coated Fe_3O_4 NPs were washed by three alternate cycles of centrifuging and resuspending the particles in pure water. PLL solution (1 mL, $1\,mg\,mL^{-1}$, pH 7.4 PBS buffer that contained 0.5 M NaCl) was then added into the PGA-modified Fe_3O_4 NP suspension and purified in the same manner. These steps were repeated until 5 layers, $(PGA/PLL)_2PGA$, were deposited onto the Fe_3O_4 NPs. The outermost layer of FI- and FA-functionalized generation 5 PAMAM dendrimers (G5.NH_2-FI-FA) ($1\,mg\,mL^{-1}$, pH 7.4 PBS buffer that contained 0.5 M NaCl) was then deposited in the same way and the final $(PGA/PLL)_2PGA$/G5.NH_2-FI-FA-modified Fe_3O_4 NPs were dispersed into 50×10^{-3} M MES buffer (pH = 5.5) and EDC (12–18 mg) was added to crosslink the hydroxy groups of the Fe_3O_4 NPs and the amino groups of PLL and the dendrimers with the carboxy groups of PGA. The mixture was shaken overnight, followed by three cycles of centrifugation/redispersion (in water) to remove residual reactants. The SCIO NPs with FA modification (SCIO-FA NPs) were subjected to an acetylation reaction to neutralize the remaining amine groups of the G5.NH_2-FI-FA dendrimers, using a procedure described elsewhere [48]. The control SCIO NPs ($Fe_3O_4/(PGA/PLL)_2/PGA$/G5.NHAc-FI NPs) without FA conjugation (SCIO-NonFA NPs) were prepared in the same manner as the procedure used to prepare SCIO-FA NPs. The

FI-modified amine-terminated G5 dendrimers (G5.NH_2-FI) used were prepared and characterized according to a previous report [35].

General Characterization Methods: FT-IR spectra were acquired using a Perkin Elmer Spectrum GX FTIR system. Dry particles were mixed with milled KBr crystals and the samples were pressed as pellets before measurement. The iron concentration of the Fe_3O_4 NPs before and after surface modification was determined by inductively coupled plasma–optical emission spectroscopy (ICP-OES) using a Perkin–Elmer Optima 2000 DV. The surface potential of functionalized Fe_3O_4 NPs was measured by a Malvern Zetasizer Nano ZS model ZEN3600 (Worcestershire, UK) equipped with a standard 633 nm laser. The size and morphology of the Fe_3O_4 NPs were characterized by a Philips CM-100 TEM equipped with a Hamamatsu Digital Camera ORCA-HR operated using AMT software (Advanced Microscopy Techniques Corp, Danver, MA). The operation voltage was kept at 60 kV. TEM samples were prepared by deposition of a dilute particle suspension (5 μL) onto a carbon-coated copper grid and were air-dried before measurement. Stained specimens were prepared by depositing the sample solutions on the grid and inverting the grid on a drop of aqueous phosphotungstic acid solution. In order to investigate the morphology of the polymer hollow capsules before and after EDC crosslinking, the SCIO NPs were exposed to 3 M HCl to erode the Fe_3O_4 core particles. MR relaxometry of SCIO NPs was performed using a 2.0 T Varian Unity/Inova system (Palo Alto, CA) using home-built RF coils. SCIO NPs were diluted in water at variable concentrations. For MR relaxometry measurements, SCIO NPs (1 mL) were placed in 1.5 mL Eppendorf vials. T_2 relaxation times were measured using a standard CPMG pulse sequence (TR = 2000 ms, TE range 30–960 ms, 32 echoes, FOV = 134×67 mm^2, matrix 128×64, slice thickness 10 mm, BW = 40, NEX = 3). T_2 relaxation times were calculated by a linear fit of the logarithmic ROI signal amplitudes versus TE. The T_2 relaxivities ($r2$) were determined by a linear fit of the inverse relaxation times as a function of the Fe concentration used.

KB Cell Culture: The KB cells were continuously grown in two 24-well plates, one in FA-free medium and the other in regular RPMI 1640 medium supplemented with penicillin (100 units mL^{-1}), streptomycin (100 μg mL^{-1}), 10% heat-inactivated fetal bovine calf serum (FBS), and 2.5×10^{-6} M FA. The cells grown in FA-free medium express high-level FAR, while the cells grown in FA-containing medium express low-level FAR.

Determination of Cell Viability: Cell viability was measured by FDA and PI staining. FDA stains live cells, while PI stains dead cells. The stained cells were quantified by flow cytometry as described by Killinger et al. . [49] Briefly, 2×10^5 KB cells per well were seeded into a 24-well plate and incubated with 0–100 μg mL^{-1} of unmodified Fe_3O_4 NPs, SCIO-NonFA NPs, and SCIO-FA NPs for 24 h at 37 °C. Ten thousand cells were acquired from each sample for flow cytometric analysis.

Determination of Binding Affinity by Flow Cytometry: Approximately 2×10^5 cells per well were seeded in 24-well plates the day before the experiments. An hour before initiating an experiment, the cells were rinsed three times with serum-free and FA-deficient RPMI 1640 medium. SCIO-NonFA and SCIO-FA NPs were added at Fe concentrations of 0–50 μg mL^{-1}. After 1 h of incubation at 37 °C, KB cells with both high- and low-level FAR were trypsinized and suspended in PBS that contained 0.1% bovine serum albumin, and then analyzed using a Coulter EPICS-XL MCL Beckman–Coulter flow cytometer. The FL1-fluorescence of 10 000 cells was measured, and the mean fluorescence of gated viable cells was quantified using Expo32 software (Beckman–Coulter, Miami, FL).

In-vitro MR Relaxometry and Imaging: KB-HFAR cells (5×10^6) were incubated with SCIO-NonFA and SCIO-FA NPs with Fe concentrations of 6.3, 12.5, and 25 μg mL^{-1} for 30 min in an ice bath. Live cells were usually cultured with a complete medium at 37 °C. For the MR imaging studies, live cells were trypsinized and suspended in PBS (instead of cell culture medium) and incubated with NPs. The cells were then washed with PBS buffer three times. The cells were centrifuged to prepare pellets for MR imaging according to the procedure described in a previous report [35].

Tumor Model: A murine tumor model was established in NOD C.B-17 SCID mice using human KB tumor cells over-expressing FAR as described previously [18]. When the tumor nodules had reached a volume of 0.60 ± 0.15 cm^3 (approximately 3 weeks post-injection), the animals were randomly allocated into control, SCIO-NonFA, and SCIO-FA groups. SCIO-FA and SCIO-NonFA NPs were delivered via the tail vein in 0.1 mL of saline at 12.4 μg Fe per mouse, respectively. Two-dimensional (2D) and three-dimensional (3D) MR images were obtained both before and after administration of either imaging agent at time points of hours 1, 4, 8, 24, 48, and day 7 after injection.

In-vivo MR Imaging: The MR imaging probe, constructed specifically for these studies, was based on an Alderman–Grant slotted cylinder design (length 10 cm, OD 4.5 cm). The probe was made with polycarbonate tubing, copper tape, and ATC and Johanson capacitors. Following induced anesthesia, the mouse to be imaged was placed inside a second polycarbonate tube (ID 2.6 cm). This second tube was then inserted into the MR probe, which allowed easy animal positioning and restricted the mouse MR imaging studies to a region of homogeneous RF field. MR imaging was performed on a 2T Varian Unity/Inova system equipped with Acustar S180 gradients. At each time point for each animal, 2D and 3D gradient-echo MR images were obtained. Two sets of interleaved, 2D gradient-echo images were acquired with a 2 mm slice thickness, TR/TE 100/5 ms, flip angle 45°, in plane resolution 390 mm, and 8 averages. The total time to acquire the 2D images was 2.5 min. The 3D gradient-echo images were acquired with a TR/TE of 20/4 ms, a flip angle of 20°, isotropic voxel resolution of 390 mm, and 4 averages. Imaging time for the 3D dataset was 5.5 min. The 3D gradient echo pulse sequence was chosen to provide isotropic spatial resolution, minimize motion artifacts, and generate T_2-weighted MR images. See Supporting Information for details.

Received: November 7, 2007
Revised: December 14, 2007
Published online: April 11, 2008

[1] A. Moore, L. Josephson, R. M. Bhorade, J. P. Basilion, R. Weissleder, *Radiology* **2001**, *221*, 244.
[2] Z. M. Qian, H. Li, H. Sun, K. Ho, *Pharmacol. Rev.* **2002**, *54*, 561.
[3] F. Hu, L. Wei, Z. Zhou, Y. Ran, Z. Li, M. Gao, *Adv. Mater.* **2006**, *18*, 2553.
[4] Y.-M. Huh, Y.-W. Jun, H.-T. Song, S. Kim, J.-S. Choi, J.-H. Lee, S. Yoon, K.-S. Kim, J.-S. Shin, J.-S. Suh, J. Cheon, *J. Am. Chem. Soc.* **2005**, *127*, 12387.
[5] J. H. Lee, Y. M. Huh, Y. W. Jun, J. W. Seo, J. T. Jang, H. T. Song, S. Kim, E. J. Cho, H. G. Yoon, J. S. Suh, J. Cheon, *Nat. Med.* **2007**, *13*, 95.
[6] I. Hilger, R. Trost, J. R. Reichenbach, W. Linß, M.-R. Lisy, A. Berndt, W. A. Kaiser, *Nanotechnology* **2007**, *18*, 135103.
[7] O. Veiseh, C. Sun, J. Gunn, N. Kohler, P. Gabikian, D. Lee, N. Bhattarai, R. Ellenbogen, R. Sze, A. Hallahan, J. Olson, M. Zhang, *Nano Lett.* **2005**, *5*, 1003.
[8] D. Weitman, R. H. Lark, L. R. Coney, D. W. Fort, V. Frasca, V. R. Surawski, B. A. Kamen, *Cancer Res.* **1992**, *52*, 3396.
[9] J. F. Ross, P. K. Chaudhuri, M. Ratnam, *Cancer* **1994**, *73*, 2432.
[10] I. G. Campbell, T. A. Jones, W. D. Foulkes, J. Trowsdale, *Cancer Res.* **1991**, *51*, 5329.
[11] N. Kohler, G. E. Fryxell, M. Zhang, *J. Am. Chem. Soc.* **2004**, *126*, 7206.
[12] F. Sonvico, S. Mornet, S. Vasseur, C. Dubernet, D. Jaillard, J. Degrouard, J. Hoebeke, E. Duguet, P. Colombo, P. Couvreur, *Bioconjugate Chem.* **2005**, *16*, 1181.
[13] C. Sun, R. Sze, M. Zhang, *J. Biomed. Mater. Res, A* **2006**, *78A*, 550.
[14] Y. Zhang, N. Kohler, M. Zhang, *Biomaterials* **2002**, *23*, 1553.
[15] Y. Zhang, C. Sun, N. Kohler, M. Zhang, *Biomed. Microdevices* **2004**, *6*, 33.

ADVANCED MATERIALS

[16] S. Mohapatra, S. K. Mallick, T. K. Maiti, S. K. Ghosh, P. Pramanik, *Nanotechnology* **2007**, *18*, 385102.
[17] S. C. Wuang, K. G. Neoh, E.-T. Kang, D. W. Pack, D. E. Leckband, *J. Mater. Chem.* **2007**, *17*, 3354.
[18] J. F. Kukowska-Latallo, K. A. Candido, Z. Cao, S. S. Nigavekar, I. J. Majoros, T. P. Thomas, L. P. Balogh, M. K. Khan, J. R. Baker, Jr., *Cancer Res.* **2005**, *65*, 5317.
[19] I. J. Majoros, A. Myc, T. P. Thomas, C. B. Mehta, J. R. Baker, Jr., *Biomacromolecules* **2006**, *7*, 572.
[20] I. J. Majoros, T. P. Thomas, C. B. Mehta, J. R. Baker, Jr., *J. Med. Chem.* **2005**, *48*, 5892.
[21] T. P. Thomas, I. J. Majoros, A. Kotlyar, J. F. Kukowska-Latallo, A. Bielinska, A. Myc, J. R. Baker, Jr., *J. Med. Chem.* **2005**, *48*, 3729.
[22] X. Shi, T. P. Thomas, L. A. Myc, A. Kotlyar, J. R. Baker, Jr., *Phys. Chem. Chem. Phys.* **2007**, *9*, 5712.
[23] G. Decher, *Science* **1997**, *277*, 1232.
[24] F. Caruso, R. A. Caruso, H. Mohwald, *Science* **1998**, *282*, 1111.
[25] E. Donath, G. B. Sukhorukow, F. Caruso, S. A. Davis, H. Möhwald, *Angew. Chem. Int. Ed.* **1998**, *37*, 2201.
[26] G. Schneider, G. Decher, *Nano Lett.* **2004**, *4*, 1833.
[27] G. Schneider, G. Decher, N. Nerambourg, R. Praho, M. H. V. Werts, M. Blanchard-Desce, *Nano Lett.* **2006**, *6*, 530.
[28] D. I. Gittins, F. Caruso, *Adv. Mater.* **2000**, *12*, **1947**.
[29] D. I. Gittins, F. Caruso, *J. Phys. Chem. B* **2001**, *105*, 6846.
[30] A. F. Thunemann, D. Schutt, L. Kaufner, U. Pison, H. Mohwald, *Langmuir* **2006**, *22*, 2351.
[31] C. Cortez, E. Tomaskovic-Crook, A. P. R. Johnston, B. Radt, S. H. Cody, A. M. Scott, E. C. Nice, J. K. Heath, F. Caruso, *Adv. Mater.* **2006**, *18*, **1998**.
[32] N. Kato, F. Caruso, *J. Phys. Chem. B* **2005**, *109*, 19604.
[33] D. Wang, A. L. Rogach, F. Caruso, *Nano Lett.* **2002**, *2*, 857.
[34] B. Thierry, S. Faghihi, L. Torab, G. B. Pike, M. Tabrizian, *Adv. Mater.* **2005**, *17*, 826.
[35] S. Wang, X. Shi, M. Van Antwerp, Z. Cao, S. D. Swanson, X. Bi, J. R. Baker, Jr., *Adv. Funct. Mater.* **2007**, *17*, 3043.
[36] W. Tong, C. Gao, H. Mohwald, *Chem. Mater.* **2005**, *17*, 4610.
[37] W. Tong, C. Gao, H. Mohwald, *Macromolecules* **2006**, *39*, 335.
[38] P. Schuetz, F. Caruso, *Adv. Funct. Mater.* **2003**, *13*, 929.
[39] I. Pastoriza-Santos, B. Scholer, F. Caruso, *Adv. Funct. Mater.* **2001**, *11*, 122.
[40] C. Picart, R. Elkaim, L. Richert, F. Audoin, Y. Arntz, M. Da Silva, P. Cardoso, J.-C. Schaaf, B. Frisch. Voegel, *Adv. Funct. Mater.* **2005**, *15*, 83.
[41] C. Picart, A. Schneider, O. Etienne, J. Mutterer, P. Schaaf, C. Egles, N. Jessel, J.-C. Voegel, *Adv. Funct. Mater.* **2005**, *15*, 1771.
[42] T. J. Halthur, U. M. Elofsson, *Langmuir* **2004**, *20*, 1739.
[43] P. Lavalle, C. Gergely, F. J. G. Cuisinier, G. Decher, P. Schaaf, J. C. Voegel, C. Picart, *Macromolecules* **2002**, *35*, 4458.
[44] P. Tryoen-Toth, D. Vautier, Y. Haikel, J.-C. Voegel, P. Schaaf, J. Chluba, J. Ogier, *J. Biomed. Mater. Res.* **2002**, *60*, 657.
[45] X. Shi, A. L. Briseno, R. J. Sanedrin, F. Zhou, *Macromolecules* **2003**, *36*, 4093.
[46] C. Zhang, B. Wangler, B. Morgenstern, H. Zentgraf, M. Eisenhut, H. Untenecker, R. Kruger, R. Huss, C. Seliger, W. Semmler, F. Kiessling, *Langmuir* **2007**, *23*, 1427.
[47] Y.-W. Jun, Y.-M. Huh, J.-S. Choi, J.-H. Lee, H.-T. Song, S.-J. Kim, S. Yoon, K.-S. Kim, J.-S. Shin, J.-S. Suh, J. Cheon, *J. Am. Chem. Soc.* **2005**, *127*, 5732.
[48] I. J. Majoros, B. Keszler, S. Woehler, T. Bull, J. R. Baker, Jr., *Macromolecules* **2003**, *36*, 5526.
[49] W. A. Killinger, Jr., D. B. Dorofi, E. A. Tinsley, Jr., B. A. Keagy, G. Johnson, Jr., *Ann. Thorac. Surg.* **1992**, *53*, 472.